Sensors & Actuators: B. Chemical 309 (2020) 127768

Contents lists available at ScienceDirect

Sensors and Actuators B: Chemical

journal homepage: www.elsevier.com/locate/snb

Pyrochlore Ca-doped $Gd_2Zr_2O_7$ solid state electrolyte type sensor coupled with ZnO sensing electrode for sensitive detection of HCHO

Li Jiang[a], Caileng Wang[a], Jing Wang[a], Fangmeng Liu[a,*], Rui You[b], Siyuan Lv[a], Guoyan Zeng[a], Zijie Yang[a], Junming He[a], Ao Liu[a], Xu Yan[a], Peng Sun[a], Jie Zheng[a], Geyu Lu[a,*]

[a] State Key Laboratory of Integrated Optoelectronics, Key Laboratory of Advanced Gas Sensors, Jilin Province, College of Electronic Science and Engineering, Jilin University, 2699 Qianjin Street, Changchun 130012, China
[b] Institute of Microelectronics, Peking University, Beijing 100871, China

ARTICLE INFO

Keywords:
HCHO sensor
Pyrochlore solid electrolyte
Ca-doped $Gd_2Zr_2O_7$
Rod-shaped ZnO

ABSTRACT

Solid state electrolyte type formaldehyde (HCHO) gas sensors based on a novel pyrochlore structure $Gd_2Zr_2O_7$ solid electrolyte coupled with rod-shaped ZnO sensing electrode (SE) were initially designed and fabricated in this paper. The incorporation of alkaline-earth metal Ca can significantly improve sensing performance of the $Gd_2Zr_2O_7$ based sensors to HCHO. The response value (ΔV) of the sensors based on $Gd_{2-x}Ca_xZr_2O_7$ (x = 0, 0.02, 0.05 and 0.1) varied approximately linear with the logarithm of HCHO concentration in the range of 1 − 100 ppm at 600 °C, with sensitivities of -25, -30, -15 and -5 mV/decade, respectively. The optimal sensor based on $Gd_{1.98}Ca_{0.02}Zr_2O_7$ (GCZ(0.02)) exhibited the excellent sensing characteristics with maximum response value (-61.3 mV) and extremely short response time (3 s) to 100 ppm HCHO. In addition, the GCZ(0.02) sensor also showed good selectivity and stability within 20-day period of continuous high-temperature aging under high-humidity condition. Conclusively, the sensing behavior and mechanism based on mixed potential were investigated and demonstrated by the mearsurement of the polarization curves.

1. Introduction

In recent decades, indoor air quality issues have increasingly become the focus of public attention with the improvement of living standards and human consciousness. Among multitudinous indoor harmful gases, formaldehyde (HCHO), primarily comes from various decoration materials, is becoming the top killer to human health [1–4]. The main harm of HCHO is the stimulation that it to the skin mucosa and respiratory tract. People who have been exposed to high concentrations of HCHO gas for a long time have a greater risk of suffering cancer. Mild discomfort caused by HCHO includes symptoms such as cough, headache, fatigue, and more serious is that HCHO can induce tumors and even death [5–8]. At the same time, as an irreplaceable material, HCHO also has a wide range of applications in the field of textile, wood and other industries, which increases the chances of people coming into contact with it [9]. Therefore, it is extremely urgent and necessary to detect HCHO through rapid, portable and efficient methods.

Generally, methods for detecting HCHO include chromatography, fluorescence spectrophotometry, gas sensors and so on [10–15]. Thereinto, gas sensors are widely developed and applied due to the advantages of low cost, miniaturization, portability, real-time and effectively detection. The solid state electrolyte type gas sensors for monitoring various gases, such as NO_x, NH_3, SO_2, Triethylamine, VOCs, have been largely investigated and developed in different applications [16–21]. However, the development of solid electrolyte type sensor for detection of HCHO is rarely reported or even stagnation. Inspired by above-mentioned works, the development of more stable solid state electrolyte sensors will have a great significance in the field of HCHO detection, and the selection of solid electrolyte and sensing electrode is the primary consideration.

Recently, a novel solid electrolyte with pyrochlore structure has shown great application prospects in the field of gas sensors because of its large concentration of intrinsic oxygen vacancy [22–25]. Pyrochlore-phase solid electrolyte usually has a general chemical formula of $A_2B_2O_7$, where A and B can be either trivalent and tetravalent or divalent and pentavalent metallic cations, respectively [26]. In the series of pyrochlore $A_2B_2O_7$ compounds, $Gd_2Zr_2O_7$ is the most widely studied substance. Fig. 1 shows the coordination structure of Gd^{3+} and Zr^{4+} in $Gd_2Zr_2O_7$ crystal [27]. It can be seen that each Zr^{4+} is coordinated with the surrounding 8 O atoms (6 O-48f and 2 O-8b), whereas there are only 6 O-48f around each of Gd^{3+} and the concentration of intrinsic oxygen

* Corresponding authors.
E-mail addresses: liufangmeng@jlu.edu.cn (F. Liu), lugy@jlu.edu.cn (G. Lu).

https://doi.org/10.1016/j.snb.2020.127768
Received 21 October 2019; Received in revised form 12 January 2020; Accepted 21 January 2020
Available online 22 January 2020
0925-4005/

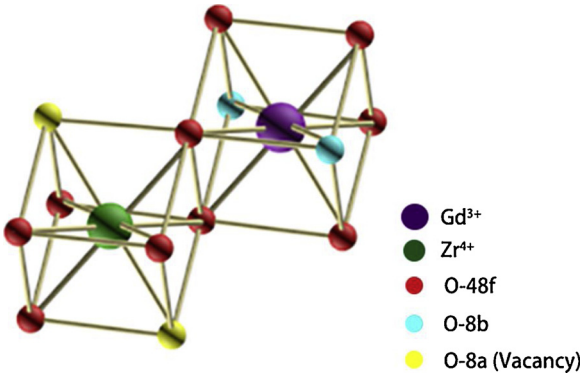

Fig. 1. Coordination structure of Gd^{3+} and Zr^{4+} in pyrochlore $Gd_2Zr_2O_7$ crystal.

vacancies (O-8a) reaches 12.5 %. In $Gd_2Zr_2O_7$ compound, the value of r $(Gd^{3+})/r(Zr^{4+})$ is the minimum of the prerequisite for the formation of pyrochlore structure, which means that it may have a higher conductivity compared to other substances, but on the other hand it may also cause instability of the structure. A small amount of metal doping might be possible to mitigate this effect [26–31]. Inspired by the previous studies on solid electrolyte type gas sensors [32,33], here, we considered the effcct caused by partial Ca doping into the Gd position and prepared the $Gd_{2-x}Ca_xZr_2O_7$ (GCZ(x)) solid electrolytes.

The selection of sensing electrode material is another consideration for the development of solid electrolyte sensors. In the past few decades, a large number of metal oxides [34–37], such as NiO [38], ZnO [39,40], $CoTiO_3$ [41], $CoNb_2O_6$ [42], have been developed to detect a variety of pollutant gases. Among them, ZnO was found to have good sensitivity to HCHO, and a lot of work for ZnO modification has been devoted to optimize the sensing performance [43–46].

In this work, pyrochlore $Gd_{2-x}Ca_xZr_2O_7$ based solid electrolyte type gas sensors coupled with ZnO sensing material were firstly fabricated. The detailed gas sensing performance and sensing mechanism to HCHO were investigated and proposed.

2. Experimental

2.1. Synthesis and characterization of the $Gd_{2-x}Ca_xZr_2O_7$ solid electrolyte

The main synthetic steps of the electrolyte are referenced in the literature [30]. Specifically, the $Gd_{2-x}Ca_xZr_2O_7$ (x = 0, 0.02, 0.05 and 0.1) solid electrolyte materials were prepared through facile hydrothermal synthesis followed by high temperature sintering at 1500 °C. Firstly, fixed amount of $Gd(NO_3)_3{\cdot}6H_2O$, $Ca(NO_3)_2{\cdot}2H_2O$ and $ZrOCl_2{\cdot}8H_2O$ materials were dissolved in 40 mL deionized water to form a mixed solution with total cation concentration of 0.25 mol/L.Then, 25 mmol urea as precipitant was added into above-obtained solution with magnetic stirrerring for 30 min to form a thorough mixed solution. After that the solution was transferred into a Teflon-lined autoclave (100 mL), sealed and removed into an oven with controlling temperature at 180 °C for 24 h. After the autoclave was cooled to room temperature, white precipitates were separated by centrifugation, alternately washed with deionized water and ethanol for 6 times, then dried at 80 °C for 24 h in drying oven to obtain white powder. After the obtained powder was pre-sintered at 600 °C for 4 h, a small portion was directly sintered at 1500 °C for 4 h to characterize the structure of the material. The remaining was unidirectionally pressed into a pellet (φ10 mm * 2 mm) under a pressure of 280 Mpa for 5 min and then sintered at 1500 °C for 4 h as solid electrolyte substrate of gas sensor [30,38,55].

The crystalline and molecular structure of $Gd_{2-x}Ca_xZr_2O_7$ were identified by X-ray diffraction (XRD) using Rigaku wide-angle X-ray diffractometer (D/max rA, using Cu Kα radiation at wave length = 0.1541 nm) in the angle (2θ) range of 5-70° and Raman spectroscopy (LabRAM HR Evolution, Jobin-Yvon, Horiba, France) in the range of 200-1000 cm^{-1} excited by a He-Ne laser with a wavelength of 532 nm. Conductivity was investigated using an impedance analyzer (Solartron 1260 and Solartron 1287) with the amplitude of the AC potential signal at 50 mV within the frequency range of 10 MHz-0.1 Hz at 500 − 800 °C.

2.2. Synthesis and characterization of rod-shaped ZnO sensing electrode

The rod-shaped ZnO sensing material was prepared based on hydrothermal method. 0.2 g $ZnCl_2{\cdot}2H_2O$ and 2 g Na_2CO_3 dissolved in 40 mL deionized water and reacted in an oven of 110 °C for 12 h. Obtained products were then sintering at 800 °C for 4 h.

The crystal phase was analyzed by Rigaku wide-angle X-ray diffractometer (D/Max rA, using Cu Kα radiation at wave length = 0.1541 nm) in the 2θ range of 5-80°. The microstructure was observed by Field-Emission Scanning Electron Microscopy (JEOL JSM-6500 F, Accelerating voltage = 15 kV) and Transmission Electron Microscopy (TEM; JEM 2100 F, Accelerating voltage = 200 kV). The element spot pattern scanning analysis was tested by Energy-Dispersive X-ray Spectroscopy (EDS).

2.3. Fabrication and measurement of solid electrolyte type gas sensors

First, $Gd_{2-x}Ca_xZr_2O_7$ (x = 0, 0.02, 0.05 and 0.1) solid electrolyte pellets were cut into substartes with the physical dimensions of 2 mm * 2 mm * 0.4 mm, respectively. Second, commercial Pt paste (Sino-platinum Metals Co., Ltd) was printed on both ends of the electrolyte substartes which were wound around with two Pt wires and then sintered at 1000 °C for 0.5 h to form a striped-shaped Pt reference electrode (RE) on one end and a point-shaped Pt junction on the other. Third, ZnO sensing material was thoroughly mixed with deionized water to form paste of uniform viscosity and then was painted on the point-shaped Pt junction to form a stripe-shaped ZnO-SE. Then the device was sintered at 800 °C for 2 h to ensure a good contact between SE and electrolyte plate. Finally, the Al_2O_3 substrate with Pt heater was attached to the electrolyte plate using inorganic adhesive to provide the required operating temperature of the device. The sensing device based on $Gd_{2-x}Ca_xZr_2O_7$ (x = 0, 0.02, 0.05 and 0.1) solid electrolytes using ZnO-SE is marked as GCZ(0), GCZ(0.02), GCZ(0.05) and GCZ(0.1), respectively.The schematic illustration of the fabricated sensor is shown in Fig. 2.

A conventional static test method was used to evaluate the sensing properties of the fabricated sensors. The ZnO-SE and Pt-RE were respectively connected to the positive and negative terminals of a digital electrometer (Rigol Technologies, Inc., DM 3054, China). The potential formed at both electrodes of the device can be collected and displayed by computer conneted with electrometer. The response voltage (ΔV) of the sensor to different gases is defined as the difference between the potential values when the sensor was exposed to the tested gases (V_{gas}) and in the air (V_{air}) ($\Delta V = V_{gas} - V_{air}$). The current-voltage curves (polarization curves) of the device were obtained through the potentiodynamic method (CHI600C, Instrument Corporation of Shanghai, China).The humidity resistance was measured through preparing tested gases under different relative humidity controlling by humidity chamber (Shanghai ESPC Environment Equipment Corporation, China).

3. Results and discussion

The X-ray diffraction data of the prepared $Gd_{2-x}Ca_xZr_2O_7$ (x = 0, 0.02, 0.05 and 0.1) powders were shown in Fig. 3**(a)**. Generally, the compunds with pyrochlore phase structure display the characteristic peaks at the positions of 14°, 28°, 37°, 45°, which correspond to the (111), (311), (331) and (511) planes,respectively [38,47,48]. However, in the series of $Gd_{2-x}Ca_xZr_2O_7$ (x = 0, 0.02, 0.05 and 0.1) compunds,

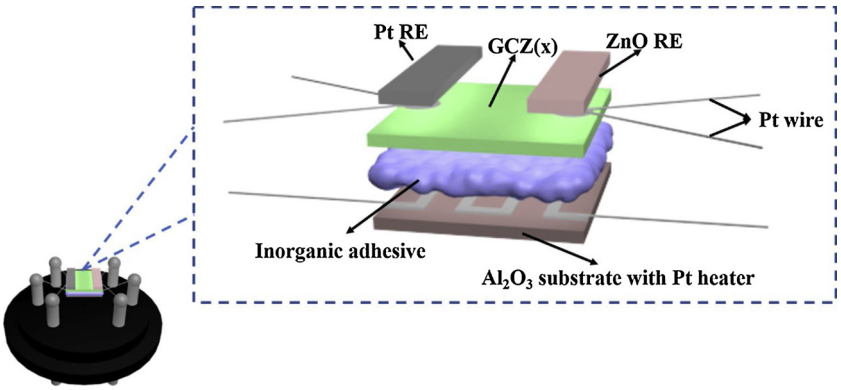

Fig. 2. Schematic illustration of the solid electrolyte type gas sensor.

there are only two peaks at 14° and 28° can be observed, and the portion of characteristic peaks in XRD datas are very weak and is difficut to be observed as it has been reported [28], thus bringing uncertainty to the determination of the structure. In order to further confirm the structures, Raman spectroscopy of the samples were performed, as shown in Fig. 3**(b)**. According to the analysis of group theory, $Gd_2Zr_2O_7$ shows six distinct bands that are $E_g + A_{1g} + 4\ F_{2g}$, where E_g and A_{1g} are considered to be the characteristic bands of the pyrochlore stucture. However, due to the overlap of several of the vibrational bands, some of those bands could not reveal [49,50]. The bands located at 310 cm^{-1} and 517 cm^{-1} are identified as the E_g mode and A_{1g} mode, respectively, and the other two bands at 412 cm^{-1} and 600 cm^{-1} are assigned to two F_{2g} modes. Specifically, the E_g mode is attributed to the mixture of the Zr-O, Gd-O stretch vibration and O-Zr-O bending vibration, the A_{1g} mode is attributed to the mixture of the Gd-O stretch vibration and O-Zr-O bending vibration, and the F_{2g} mode is assigned to Zr-O_6 bending vibration. Combined with XRD alanalysis, these results indicated that the prepared $Gd_{2-x}Ca_xZr_2O_7$ (x = 0, 0.02, 0.05 and 0.1) electrolytes possessed pyrochlore structure. Additionally, it can be observed that with the incorporation of alkaline-earth metal Ca, a new band is presented at around 718 cm^{-1}, which corresponds to the Ca−O symmetrical stretch vibration. This proves that Ca was successfully incorporated into the Gd site of $Gd_2Zr_2O_7$. Furthermore, the microstructures of $Gd_{2-x}Ca_xZr_2O_7$ samples sintered at 1500 °C for 4 h were given in Fig. S**1 (a–d)**. The samples are composed of conjoined particles with diameter of micro-scale and the doping of Ca did not significantly affect the microstructure of the samples. Fig. S**1 (e)** showed the microstructure of $Gd_{1.98}Ca_{0.02}Zr_2O_7$ pellet sintered at 1500 °C. As shown, the surface of the pellet presents non-uniform grain structure and high density with a clear boundary during the grains. This structure with high density of the electrolyte sheet is beneficial to reduce the grain boundary resistance and facilitates the ion transmission.

For GCZ(x) solid electrolytes, electrical conductivity is an important parameter for consideration. The electrical conductivity in the temperature range of 500 − 800 °C was calculated according to σ= t/(S•ρ), where t and S are the thickness and cross-sectional area of the sheet and ρ is resistance of electrolyte sheet measured using impedance analyzer, respectively. Fig. 4**(a)** showed the relationship between the conductivity and the temperature. Obviously, the conductivities increase with increasing temperature when fixing the Ca content. When the temperature raised from 500 °C to 800 °C, the conductivity rapidly increases from the order of 10^{-5} S cm^{-1} to that of 10^{-2} S cm^{-1}. Moreover, the conductivity of the electrolyte gradually decreases with the increasing of Ca doping, which may be due to the ionic radius of Ca being smaller than Gd, causesing lattice shrinkage to limit the migration of oxygen vacancies. However, after the temperature reaches 800 °C, the conductivity will be greatly improved since Ca is excited to participate in conduction. In order to further study the quantitative relationship between conductivity and temperature, the Arrhenius plots of Fig. 4**(b)** was obtained. Very good linear relationship indicates that the migration of oxygen vacancies in the series is thermally activated, and the activation energy E_a calculated from the slope in the Arrhenius plots is 0.89, 0.94, 0.86 and 0.95 eV for $Gd_2Zr_2O_7$, $Gd_{1.98}Ca_{0.02}Zr_2O_7$, $Gd_{1.95}Ca_{0.05}Zr_2O_7$ and $Gd_{1.9}Ca_{0.1}Zr_2O_7$, respectively [51].

The XRD pattern of the ZnO powder sintered at 800 °C was shown in Fig. S**2**, which is in good agreement with the standard card (JCPDS# 36-1451), indicating that the high purity ZnO sensing electrode material was prepared. As shown in Fig. 5**(a, b)**, the ZnO sensing electrode material present a rod-shaped structure with a diameter range of 0.4-0.8 μm. The alternately disordered accumulation of the sensing material forms structures with a large number of loose porous, which facilitates the migration of HCHO gas inside the sensing electrode layer. Fig. 5**(c, d)** exhibited TEM photomicrograph and partial high resolution image of rod-shaped ZnO material. The surface of the rod is relatively flat and it has a solid structure. The spacing between two adjacent crystal faces is approximately 0.28 nm, corresponding to (100) crystal faces of ZnO. In addition, the element distribution maps of O and Zn in ZnO material were observed, as shown in Fig. 5**(e, f)**.

In order to find the optimum doping ratio of Ca in pyrochlore type $Gd_{2-x}Ca_xZr_2O_7$, sensitivities of different devices to HCHO in the

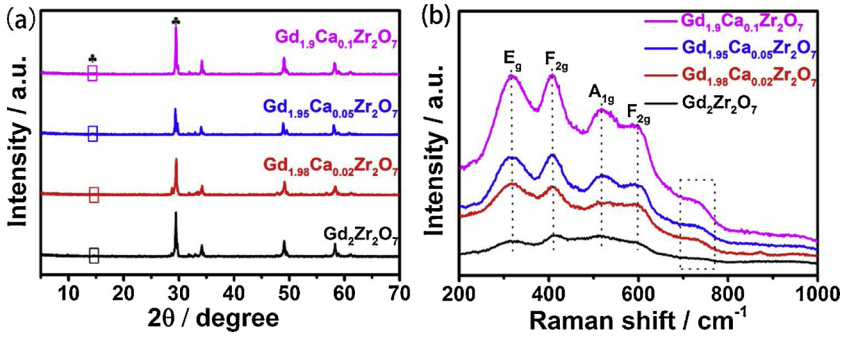

Fig. 3. XRD patterns (a) and Raman spectroscopy (b) of $Gd_{2-x}Ca_xZr_2O_7$ (x = 0, 0.02, 0.05 and 0.1) electrolyte materials sintered at 1500 °C.

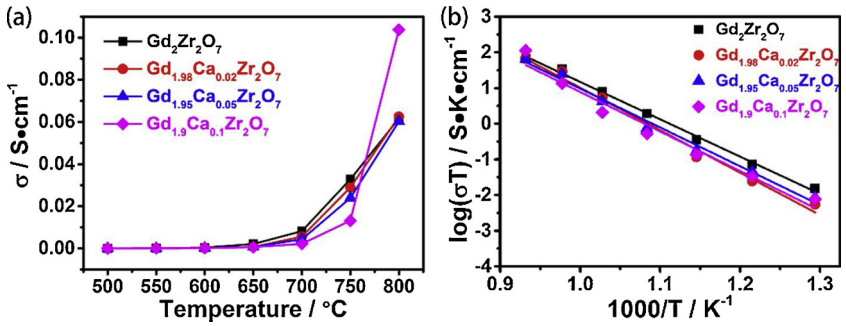

Fig. 4. (a) The dependence of the conductivity for $Gd_{2-x}Ca_xZr_2O_7$ (x = 0, 0.02, 0.05 and 0.1) at different operating temperatures; (b) Arrhenius plots of grain conductivity of $Gd_{2-x}Ca_xZr_2O_7$ (x = 0, 0.02, 0.05 and 0.1) measured in air.

concentration range of 1 − 100 ppm and the response transients toward 100 ppm HCHO at 600 °C were depicted in Fig. 6**(a, b)**, where in order to better observe the response value, the base potential levels have been shifted to 0 mV. Between ΔV and the logarithm of HCHO concentration showed liner relationship. The slope (ΔV/lgC) of the sensors based on GCZ (0, 0.02, 0.05 and 0.1) is -25, -30, -15, -5 mV/decade to 1 − 100 ppm HCHO, which is defined as the sensitivity of the sensor. Clearly, among the different sensing devices, the GCZ(0.02) sensor exhibites the highest response value to 100 ppm HCHO and the largest sensitivity to 1 − 100 ppm HCHO at 600 °C. Therefore, the optimum doping ratio of Ca is considered to be 0.02, which greatly improves the sensing characteristics to HCHO of the sensor (the characteristics of other sensing devices are shown in Fig. S**3**). The reason for this result may be that a small amount of doping improves the structure stability of the electrolyte material, but more doping causes a decrease in conductivity, which hinders the improvement of gas sensitivity. Furthermore, form Fig. 6**(c, d),** the response value of the GCZ(0.02) sensor to 100 ppm HCHO reaches -61.3 mV, and the lowest detection limit is 1 ppm with response value of -1.5 mV at 600 °C. The response and recovery times are 3 s and 13 s toward 100 ppm HCHO at 600 °C, respectively (Here we adopt the 90 % definition, that is, the response time of the sensor is the time required for potential value change arriving 90 % when the sensor is placed in the sample gas. Similarly, recovery time can also be defined). This result demonstrates that GCZ (0.02) sensor possesses rapid response and recovery capacity. The reason for linear relationship between ΔV and the logarithm of HCHO concentrations for GCZ(0.02) sensor could be explained by the mixed-potential sensing mechanism. According to previous studies, on the tripe phase boundary (TPB) of HCHO/GCZ(x)/ZnO, the electrochemical cathodic reaction of O_2 (reaction (1)) and the anodic reaction of HCHO (reaction (2)) occur simultaneously and form a local cell (*) [52–54].

(−) air + HCHO, Pt /GCZ(x)/ZnO, HCHO + air (+)(*)

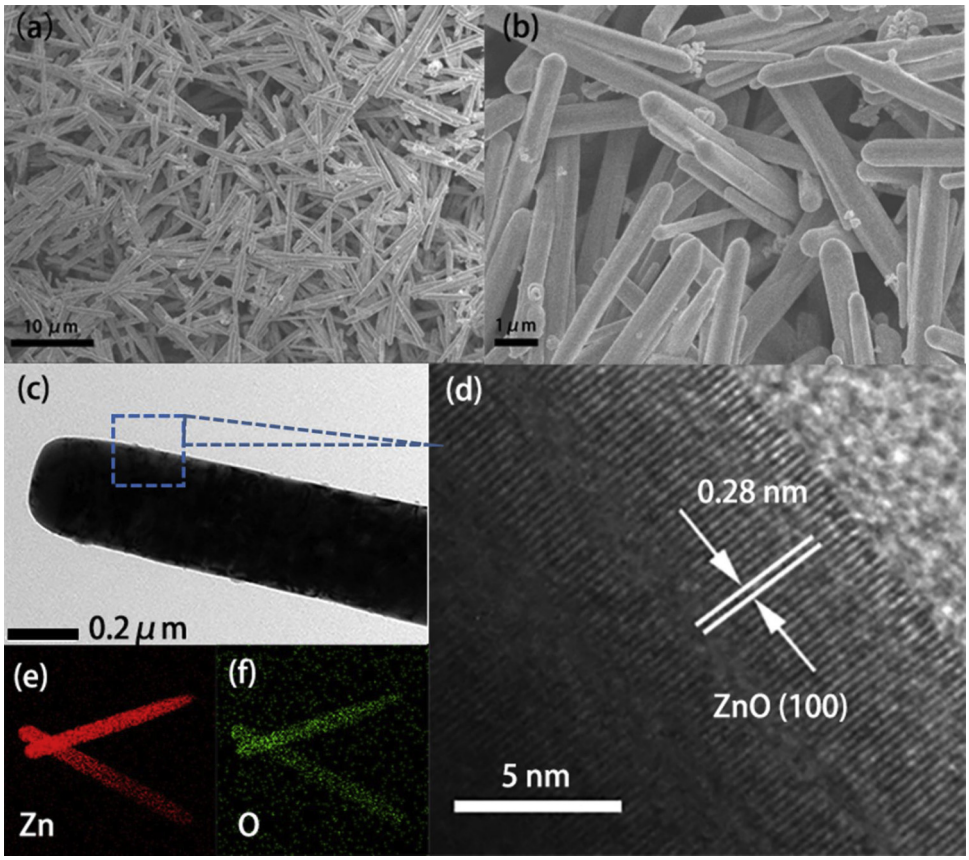

Fig. 5. (a, b) SEM images of ZnO sensing electrode material sintered at 800 °C; (c, d) TEM images and (e, f) EDS element map sanning images of ZnO sensing electrode material.

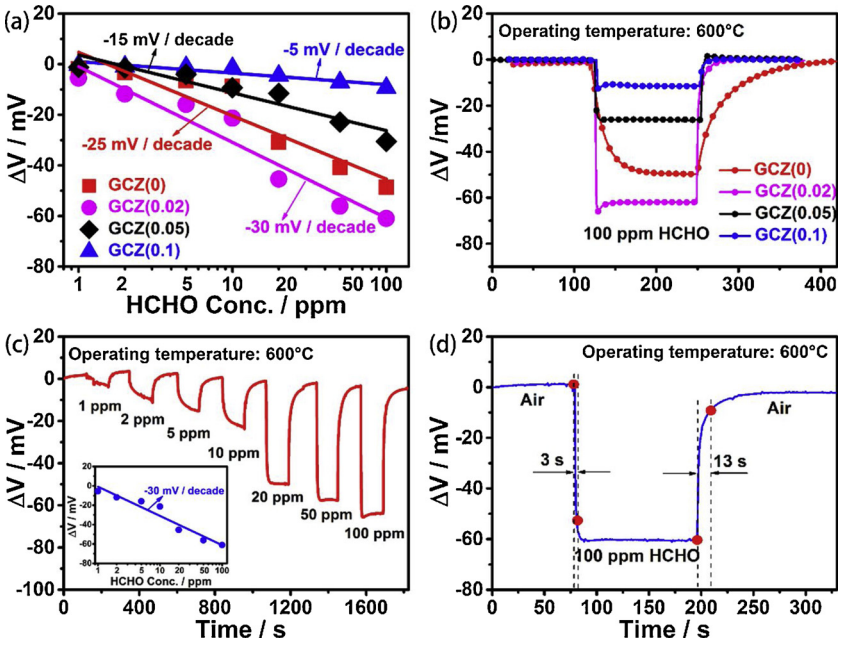

Fig. 6. (a) Sensitivities of sensing devices based on different electrolytes at 600 °C; (b) The response/recovery characteristics of sensing devices based on different electrolytes to 100 ppm HCHO at 600 °C; (c)The response transients of the GCZ(0.02) sensor to HCHO in the concentration range of 1 − 100 ppm and sensitivity at 600 °C; (d) Response and recovery characteristics of the GCZ(0.02) sensor to 100 ppm HCHO.

Cathodic reaction: $O_2 + 4e^- = 2O^{2-}$ (1)

Anodic reaction: $HCHO + 2O^{2-} = CO_2 + H_2O + 4e-$ (2)

According to Butler–Volmer Equation, the current density equations are expressed as:

$$i_{HCHO} = i^0_{HCHO}\exp[\frac{2\alpha_1 F(V - V^0_{HCHO})}{RT}] \quad (3)$$

$$i_{O_2} = i^0_{O_2}\exp[\frac{-2\alpha_2 F(V - V^0_{O_2})}{RT}] \quad (4)$$

Where,

$$i^0_{HCHO} = B_1 C^n_{HCHO},\ i^0_{O_2} = -B_2 C^m_{O_2}$$

Therein, i^0, α, F, V, V^0, R, T, and C represent the Exchange current density, Transfer coefficient, Faraday constant, Electrode potential, Equilibrium electrode potential, Gas constant, Temperature and Gas concentration, respectively; and B_1, B_2, m, n are constants. When the rates of electrochemical cathodic reaction (1) and anodic reaction (2) reach a dynamic equilibrium, that is, $i_{HCHO} + i_{O_2} = 0$ the mixed potential (V_M) is formed and can be calculated:

$$V_M = V_0 + mAlnC_{O_2} - nAlnC_{HCHO} \quad (5)$$

Where,

$$V_0 = \frac{RT}{(2\alpha_1 + 2\alpha_2)F} ln\frac{B_2}{B_1} + \frac{\alpha_1 V^0_{HCHO} + \alpha_2 V^0_{O_2}}{\alpha_1 + \alpha_2}$$

$$A = \frac{RT}{(2\alpha_1 + 2\alpha_2)F}$$

Eq. (5) can be written as follows if the O_2 concentration was a fixed value:

$$V_M = V_0 - nAlnC_{HCHO} \quad (6)$$

Therefore, the potential response value of the sensor varied negatively linear to the logarithm of HCHO concentration in the case of fixed O_2 concentration, which is in accordance with the result. The polarization curves of different sensing devices based on different electrolytes were also measured after exposed to 100 ppm HCHO at 600 °C. As shown in Fig. 7**(a)**, polarization curve of GCZ(0.02) in 100 ppm HCHO has a larger slope comparing to the other devices, indicating that GCZ (0.02) exhibited the optimal sensing characteristics because of its best electrochemical catalytic activity for HCHO. Additionly, The polarization curves of GCZ(0.02) sensor in air, 50 ppm and 100 ppm HCHO were tested and the modified polarization curves are shown in Fig. 7**(b)**. The estimated values of the sensing device for 50 ppm and 100 ppm HCHO are -53 and − 59 mV, which are very close to the observed test value of − 55 and − 61 mV. The measurement results of the polarization curves not only confirm the mechanism of the mixed potential, but also explain the best sensitivity characteristics of GCZ(0.02) from the electrochemical point of view.

In addition, it is easy to see from the above analysis that the mixed potential is also affected by the O_2 concentration. Theoretically, the potential response value of the sensor and the logarithm of O_2 concentration satisfies a positive linear relationship. The response and recovery curves of GCZ(0.02) sensor to 100 ppm HCHO in 2 vol%-21 vol% O_2 at 600 °C were measured, as shown in Fig. 8**(a)**. As the O_2 concentration increases, the response potential of the GCZ(0.02) sensor to 100 ppm HCHO gradually decreased at negative direction and changed within an acceptable range. Fig. 8**(b)** shows the dependence of the response value on the logarithm of O_2 concentrations in the range of 2 vol %-21 vol%, and the positive linear variation is very consistent with the theoretical analysis.

Generally, sensing performance of a solid state electrolyte gas sensor is closely related to its operating temperature. The response change of GCZ(0.02) sensor toward 100 ppm HCHO at 550 − 675 °C is shown in Fig. S4. Before 600 °C, the response value of GCZ(0.02) sensor gradually improved with increasing operating temperature. However, the response value decreased when the working temperature was more than 600 °C. Therefore, 600 °C could be deemed as the most appropriate operating temperature for GCZ(0.02) sensor, and the following gas sensing measurement was conducted at such an operating temperature.

Moreover, the humidity resistance of the GCZ(0.02) sensor was widely concerned and investigated. Controling by the humidity chamber (Shanghai ESPC Environment Equipment Corporation, China), 100 ppm HCHO tseted gases were prepared under different relative humidity at 22 °C. As shown in Fig. 9**(a, b)**, the response and recovery characteristics of GCZ(0.02) sensor to 100 ppm HCHO at 600 °C were measured under realtive humidity of 20 %, 40 %, 60 %, 80 % and 98 %, respectively. The GCZ(0.02) sensor demostrated good response and recovery characteristics to 100 ppm HCHO in the range of 20 %–98 % RH and the response value fluctuated slightly at 600 °C. The amplitude of variation of the response value for the GCZ(0.02) sensor to 100 ppm

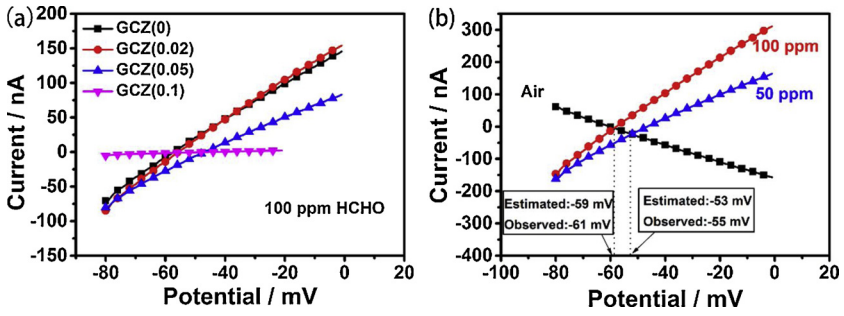

Fig. 7. (a) Polarization curves of different sensing devices in 100 ppm HCHO; (b) Polarization curves of GCZ(0.02) in different concentrations of HCHO.

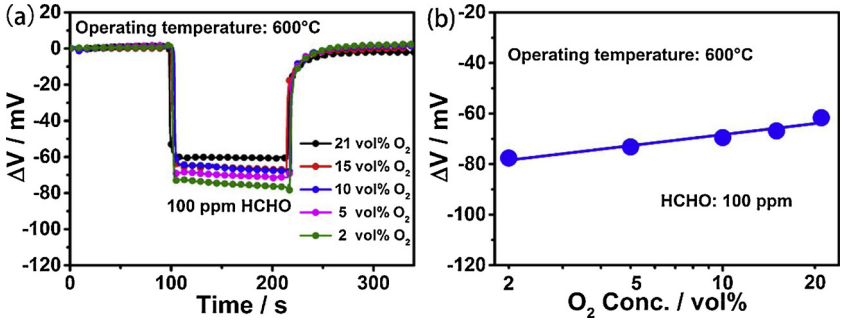

Fig. 8. (a) Response and recovery curves of GCZ(0.02) sensor to 100 ppm HCHO in 2 vol%-21 vol% O_2 at 600 °C; (b) Dependence of the response value on the logarithm of O_2 concentrations.

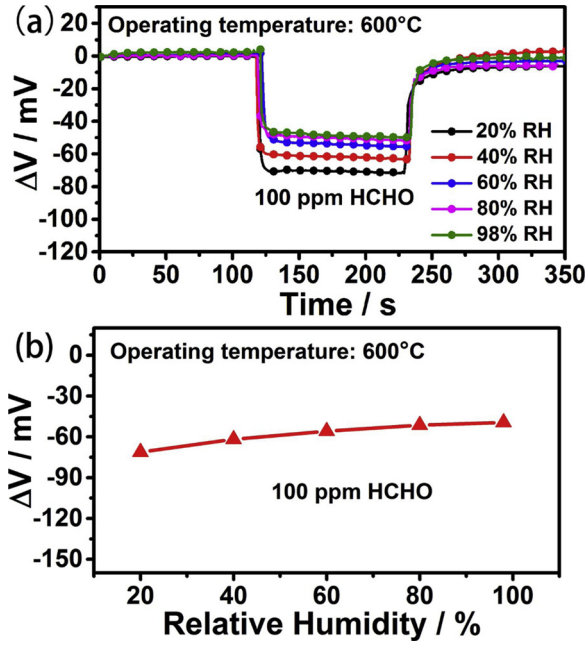

Fig. 9. (a) Response and recovery curves of GCZ(0.02) sensor to 100 ppm HCHO under 20 %–98 % RH at 600 °C; (b) Variation of response value for the sensor to 100 ppm HCHO at different relative humidity.

HCHO in 20 % RH and 98 % RH at 600 °C was 12.5 % and -19.1 %.

Actual working environment might include various coexist gases, so it is necessary to evaluate the selectivity of the developed sensor in more variable conditions with other coexist gases. The cross-sensitivities to various gases for the GCZ(0.02) sensor at 550 °C, 600 °C, 650 °C is exhibited in Fig. 10 (the concentration of each gas is 100 ppm). It is observed that GCZ(0.02) sensor displayed excellent sensitivity and selectivity to HCHO under whole of different operating temperatures, outdistancing to other tested interfering gases.

To inspect the actual application potential in HCHO detection, the

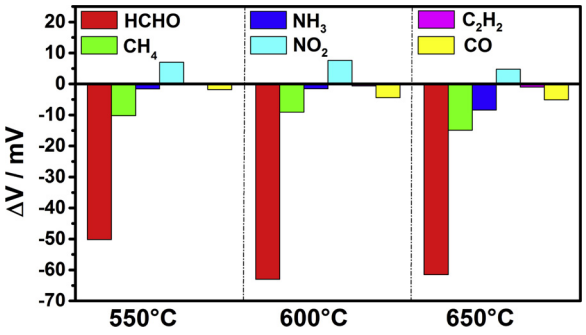

Fig. 10. Selectivity of GCZ(0.02) sensor in 100 ppm various gases at 550, 600 and 650 °C.

long-term stability of the GCZ(0.02) sensor was evaluated. The fabricated sensor operated consecutively in air at the operating temperature of 600 °C for 20 days and the response characteristics to 100 ppm HCHO were obtained through testing every few days under 60 % RH condition. It can be clearly observed from Fig. 11**(a)** that the baseline of GCZ (0.02) sensor revealed the slightly. During the consecutive 20 days, the maximum deviation of the baseline value from its average is only -16.5 % and the stability of baseline is within an acceptable range. The response and recovery transients of the sensor to 100 ppm HCHO under 60 % RH within the 20 consecutive days are present in the Fig. 11**(b)**. As indicated in Fig. 11**(b)**, the response characteristics of the sensor to 100 ppm HCHO on initial, 5th, 10th and 20th day exhibited relative good concordance at 600 °C. Furthermore, the fluctuation of ΔV (ΔV_s) for the sensor to 100 ppm HCHO is given according to $\Delta V_s = \frac{\Delta V_n - \Delta V_0}{\Delta V_0} \times 100\%$, where ΔV_0 and ΔV_n represent the response value ΔV of the sensor on the initial and nth day, respectively. The attenuation amplitude of response value for the GCZ(0.02) sensor to 100 ppm HCHO at 600 °C on 5th, 10th and 20th day were -9.4 %, -6.3 % and -11.2 %, respectively, indicating that the fabricated GCZ(0.02) sensor displayed good stability during the consecutive 20-day measurement period.

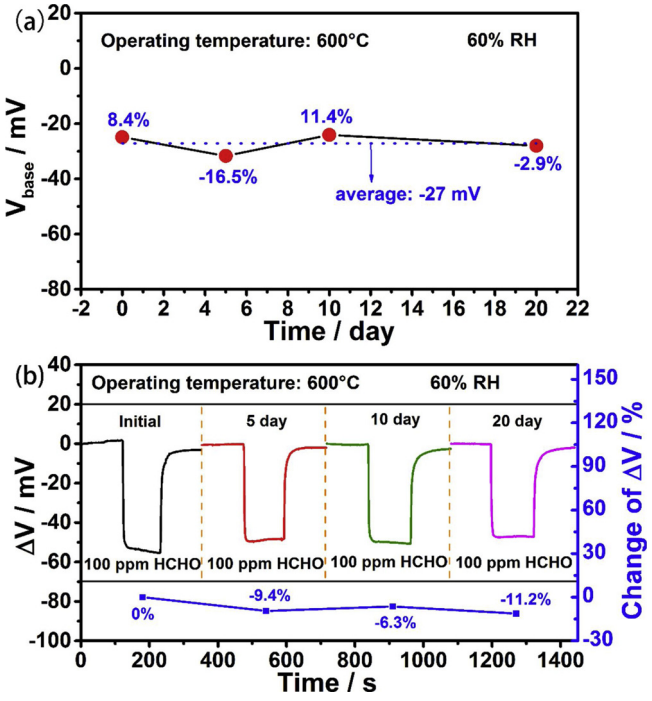

Fig. 11. Long-term stability of GCZ(0.02) sensor: (a) The changes of the baseline; (b) The response and recovery transients of GCZ(0.02) sensor to 100 ppm HCHO within the consecutive 20 days.

4. Conclusion

For the first time, pyrochlore structure $Gd_{2-x}Ca_xZr_2O_7$ solid electrolyte type gas sensors attached with rod-shaped ZnO-SE synthesized by a facile hydrothermal method are used in the field of HCHO detection. Among GCZ(0, 0.02, 0.05 and 0.1) sensors, the GCZ(0.02) sensor presented the highest sensitivity (-30 mV/decade) to $1-100$ ppm HCHO and the maximum response value (-61.3 mV) to 100 ppm HCHO at 600 °C, which is mainly attributed to good conductivity of the electrolyte and high activity of electrochemical reaction to HCHO. Furthermore, the GCZ(0.02) sensor also exhibited excellent selectivity in various coexist gases, good stability within 20-day period of high-temperature and high-humidity measurement. The Ca-doped pyrochlore $Gd_2CaZr_2O_7$ material is an important potential candidate electrolyte and the $Gd_{2-x}Ca_xZr_2O_7$ solid electrolyte type gas sensors using rod-shaped ZnO-SE displays the valuable application capacity in repid and sensitive detection of HCHO.

Declaration of Competing Interest

The authors declare that they have no known competing financial interests or personal relationships that could have appeared to influence the work reported in this paper.

Acknowledgements

This work is supported by the National Nature Science Foundation of China Nos. 61831011, 61803171, 61327804, 61520106003, 61722305 and 61833006, Program for Chang Jiang Scholars and Innovative Research Team in University No. IRT13018, National Key Research and Development Program of China Nos. 2016YFC0207300 and 2016YFC0201002, Application and Basic Research of Jilin Province20130102010 JC, Young Elite Scientists Sponsorship Program by CAST2018QN RC001, Program for JLU Science and Technology Innovative Research TeamJLUSTIRT 2017TD-07, China Postdoctoral Science Foundation Funded Project No. 2018M630322, 2019T120239, Jilin Provincial Science and Technology Development Program20190103155JH, Jilin Provincial Education Department Science and Technology ProjectJJKH20190114KJ, Fundamental Research Funds for the Central Universities.

Appendix A. Supplementary data

Supplementary material related to this article can be found, in the online version, at doi:https://doi.org/10.1016/j.snb.2020.127768.

References

[1] B. Jiang, Z. Zhou, Y. Dong, W. Tao, B. Wang, J. Jiang, J. Jiang, X. Guan, Biodegradation of benzene, toluene, ethylbenzene, and o-, m-, and p-Xylenes by the newly isolated bacterium Comamonas sp. JB, Appl. Biochem. Biotechnol. 176 (2015) 1700–1708.
[2] A. Ferrero, A. Esplugues, M. Estarlich, S. Llop, A. Cases, E. Mantilla, L. Sabrina, C. Amparo, M. Enrique, B. Ferran, I. Carmen, Infants' indoor and outdoor residential exposure to benzene and respiratory health in a Spanish cohort, Environ. Pollut. 222 (2017) 486–494.
[3] Y. Rochon, M. Sitwell, Y. Cho, A study on harmonizing total ozone assimilation with multiple sensors, Atmos. Chem. Phys. 19 (2019) 9431–9451.
[4] Q. Xu, Y. Zhang, J. Mo, X. Li, Indoor formaldehyde removal by thermal catalyst: kinetic characteristics, key parameters, and temperature influence, Environ. Sci. Technol. 45 (2011) 5754–5760.
[5] S. Takahashi, K. Tsuji, K. Fujii, F. Okazaki, T. Takigawa, A. Ohtsuka, K. Iwatsuki, Prospective study of clinical symptoms and skin test reactions in medical students exposed to formaldehyde gas, J. Dermatol. 34 (2010) 283–289.
[6] A. Dean, A. Searest, D. Powell, Contact urticaria from occupational exposure to formaldehyde, Dermatitis 27 (2016) 232.
[7] M. Salkie, The prevalence of atopy and hypersensitivity to formaldehyde in pathologists, Arch. Pathol. Lab. Med. 115 (1991) 614–616.
[8] F. Wantke, M. Focke, W. Hemmer, R. Bracun, S. Wolf-Adbolvahab, M. Gotz, R. Jarisch, M. Gotz, M. Tschabitscher, M. Gann, P. Tappler, Exposure to formaldehyde and phenol during an anatomy dissecting course: sensitizing potency of formaldehyde in medical students, Allergy 55 (2000) 84–87.
[9] J. Guthrie, Imparting wet crease resistance to cotton fabrics by cross-linking with aqueous formaldehyde, Text. Res. J. 29 (1959) 834–836.
[10] Q. Li, P. Sritharathikhun, S. Motomizu, Development of novel reagent for Hantzsch reaction for the determination of formaldehyde by spectrophotometry and fluorometry, Anal. Sci. 23 (2007) 413–417.
[11] G. Li, L. Han, Determination of formaldehyde in aquatic products by a sensitive catalytic fluorescence method, Anal. Methods 6 (2014) 426–432.
[12] X. Fu, P. Yang, X. Xiao, D. Zhou, R. Huang, X. Zhang, F. Cao, J. Xiong, Y. Hu, Y. Tu, Y. Zou, Z. Wang, H. Gu, Ultra-fast and highly selective room-temperature formaldehyde gas sensing of Pt-decorated MoO_3 nanobelts, J. Alloys. Compd. 797 (2019) 666–675.
[13] A. Nasriddinov, M. Rumyantseva, A. Marikutsa, A. Gaskov, J. Lee, J. Kim, J. Kim, S. Kim, H. Kim, Sub-ppm formaldehyde detection by n-n TiO_2@SnO_2 nanocomposites, Sensors 19 (2019) 3182.
[14] L. Zhu, K. Yuan, J. Yang, H. Ma, T. Wang, X. Ji, J. Feng, A. Devi, H. Lu, Fabrication of heterostructured p-CuO/n-SnO_2 core-shell nanowires for enhanced sensitive and selective formaldehyde detection, Sens. Actuators B Chem. 290 (2019) 233–241.
[15] H. Park, S. Hong, D. Chun, S. Kang, J. Park, D. Lee, A highly susceptive mesoporous hematite microcube architecture for sustainable P-type formaldehyde gas sensors, Sens. Actuators B Chem. 287 (2019) 437–444.
[16] J. Wang, A. Liu, C. Wang, R. You, F. Liu, S. Li, Z. Yang, J. He, X. Yan, P. Sun, G. Lu, Solid state electrolyte type gas sensor using stabilized zirconia and $MTiO_3$ (M: Zn, Co and Ni)-SE for detection of low concentration of SO_2, Sens. Actuators B Chem. 296 (2019) 126644.
[17] K. Cvejin, M. Sliwa, L. Manjakkal, J. Kulawik, G. Stojanovic, D. Szwagierczak, Impedancemetric NO sensor based on YSZ / perovskite neodymium cobaltite operating at high temperatures, Sens. Actuators B Chem. 228 (2016) 612–624.
[18] F. Liu, S. Li, J. He, J. Wang, R. You, Z. Yang, L. Zhao, P. Sun, X. Yan, X. Liang, X. Chuai, G. Lu, Highly selective and stable mixed-potential type gas sensor based on stabilized zirconia and $Cd_2V_2O_7$ sensing electrode for NH_3 detection, Sens. Actuators B Chem. 279 (2019) 213–222.
[19] Y. Zhang, C. Ma, X. Yang, Y. Song, X. Liang, X. Zhao, Y. Wang, Y. Gao, F. Liu, F. Liu, P. Sun, G. Lu, NASICON-based gas sensor utilizing $MMnO_3$ (M: Gd, Sm, La) sensing electrode for triethylamine detection, Sens. Actuators B Chem. 295 (2019) 56–64.
[20] Q. Li, W. Shi, C. Zhang, D. Jiang, SO_2 non-equilibrium gas sensor based on $Na_3Zr_2Si_2PO_{12}$ solid electrolyte, J. Inorg. Mater. 33 (2018) 229–236.
[21] P. Gross, T. Jaramillo, B. Pruitt, Cyclic-voltammetry-based solid-state gas sensor for methane and other VOC detection, Anal. Chem. 90 (2018) 6102–6108.
[22] J. Sohn, M. Kim, S. Woo, The catalytic activity and surface characterization of $Ln_2B_2O_7$ (Ln = Sm, Eu, Gd and Tb; B = Ti or Zr) with pyrochlore structure as novel CH_4 combustion catalyst, Catal. Today 83 (2003) 289–297.
[23] W. Pan, S. Phillpot, C. Wan, A. Chernatynskiy, Z. Qu, Low thermal conductivity oxides, MRS Bull. 37 (2012) 917–922.
[24] W. Ren, S. Trolier-Mckinstry, C. Randall, T. Shrout, Bismuth zinc niobate pyrochlore dielectric thin films for capacitive applications, J. Appl. Phys. 89 (2001) 767–774.

[25] Z. Liu, S. Gao, J. Ouyang, X. Xia, Influence of MoO_3 doping on structure and electrical conductivity of defect fluorite-type $Gd_2Zr_2O_7$, J. Alloys. Compd. 506 (2010) 868–871.
[26] L. Fan, X. Shu, X. Lu, Y. Xie, Y. Ding, T. Duan, B. Dan, Y. Wu, Phase structure and aqueous stability of TRPO waste incorporation into $Gd_2Zr_2O_7$ pyrochlore, Cream. Int. 41 (2015) 11741–11747.
[27] J. Zhang, D. Wang, L. Lai, X. Fang, J. Xu, X. Xu, X. Zhang, J. Liu, H. Peng, X. Wang, Probing the reactivity and structure relationship of $Ln_2Sn_2O_7$ (Ln = La, Pr, Sm and Y) pyrochlore catalysts for CO oxidation, Catal. Today 327 (2019) 168–176.
[28] Z. Wang, G. Zhou, D. Jiang, S. Wang, Recent development of $A_2B_2O_7$ system transparent ceramics, J. Adv. Ceram. 7 (2018) 289–306.
[29] F. Zhao, H. Xiao, X. Bai, Z. Liu, X. Zu, Effects of Nd doping on the mechanical properties and electronic structures of $Gd_2Zr_2O_7$: a first-principles based study, J. Mater. Sci. 53 (2018) 16423–16438.
[30] F. Zhong, L. Shi, J. Zhao, G. Cai, Y. Zheng, Y. Xiao, Y. Zheng, L. Jiang, Pyrochlore $Pr_2Zr_{2-x}M_xO_7$ (M = Al, Ga, in) solid-state electrolytes: defect-mediated oxygen hopping pathways and enhanced NO_2 sensing properties, Sens. Actuators B Chem. 270 (2018) 130–139.
[31] J. Feng, B. Xiao, C. Wan, Z. Qu, Z. Huang, J. Chen, R. Zhou, W. Pan, Electronic structure, mechanical properties and thermal conductivity of $Ln_2Zr_2O_7$ (Ln = La, Pr, Nd, Sm, Eu and Gd) pyrochlore, Acta Mater. 72 (2014) 263–265.
[32] Y. Xiao, D. Wang, G. Cai, Y. Zheng, F. Zhong, A $GdAlO_3$ perovskite oxide electrolyte-based NO_x solid-state sensor, Sci. Rep. 6 (2016) 37795.
[33] R. McCauley, Structural characteristics of pyrochlore formation, J. Appl. Phys. 51 (1980) 290–294.
[34] J. Zosel, D. Franke, K. Ahlborn, F. Gerlach, V. Vashook, U. Guth, Perovskite related electrode materials with enhanced NO sensitivity for mixed potential sensors, Solid State Ion. 179 (2008) 1628–1631.
[35] Q. Diao, C. Yin, Y. Guan, X. Liang, S. Wang, Y. Liu, Y. Hu, H. Chen, G. Lu, The effects of sintering temperature of $MnCr_2O_4$ nanocomposite on the NO_2 sensing property for YSZ-based potentiometric sensor, Sens. Actuators B Chem. 177 (2013) 397–403.
[36] N. Miura, S. Zhuiykov, T. Ono, M. Hasei, N. Yamazoe, Mixed potential type sensor using stabilized zirconia and $ZnFe_2O_4$ sensing electrode for NO_x detection at high-temperature, Sens. Actuators B Chem. 83 (2002) 222–229.
[37] S. Zhuiykov, T. Ono, N. Yamazoe, N. Miura, High-temperature NO_x sensors using zirconia solid electrolyte and zinc-family oxide sensing electrode, Solid State Ion. 152 (2002) 801–807.
[38] F. Zhong, J. Zhao, L. Shi, Y. Xiao, G. Cai, Y. Zheng, J. Long, Alkaline-earth metals-doped pyrochlore $Gd_2Zr_2O_7$ as oxygen conductors for improved NO_2 sensing performance, Sci. Rep. 7 (2017) 4684.
[39] X. Chen, Y. Shen, X. Zhong, T. Li, S. Zhao, P. Zhou, C. Han, D. Wei, Y. Shen, Synthesis of ZnO nanowires/Au nanoparticles hybrid by a facile one-pot method and their enhanced NO_2 sensing properties, J. Alloys. Compd. 783 (2019) 503–512.
[40] S. Zhao, Y. Shen, X. Yan, P. Zhou, Y. Yin, R. Lu, C. Han, B. Cui, D. Wei, Complex-surfactant-assisted hydrothermal synthesis of one-dimensional ZnO nanorods for high-performance ethanol gas sensor, Sens. Actuators B Chem. 286 (2019) 501–511.
[41] J. Wang, C. Wang, A. Liu, R. You, F. Liu, S. Li, L. Zhao, R. Jin, J. He, Z. Yang, P. Sun, X. Yan, G. Lu, High-response mixed-potential type planar YSZ-based NO_2 sensor coupled with $CoTiO_3$ sensing electrode, Sens. Actuators B Chem. 287 (2019) 185–190.
[42] F. Liu, B. Wang, X. Yang, Y. Guan, R. Sun, Q. Wang, X. Liang, P. Sun, G. Lu, High-temperature stabilized zirconia-based sensors utilizing MNb_2O_6 (M: Co, Ni and Zn) sensing electrodes for detection of NO_2, Sens. Actuators B Chem. 232 (2016) 523–530.
[43] H. Tian, H. Fan, M. Li, L. Ma, Zeolitic imidazolate framework coated ZnO nanorods as molecular sieving to improve selectivity of formaldehyde gas sensor, ACS Sens. 1 (2016) 243–250.
[44] J. Sun, L. Sun, S. Bai, H. Fu, J. Guo, Y. Feng, R. Luo, D. Li, A. Chen, Pyrolyzing Co/Zn bimetallic organic framework to form p-n heterojunction of Co_3O_4/ZnO for detection of formaldehyde, Sens. Actuators B Chem. 285 (2019) 291–301.
[45] D. Liu, J. Wan, H. Wang, G. Pang, Z. Tang, Mesoporous Au@ZnO flower-like nanostructure for enhanced formaldehyde sensing performance, Inorg. Chem. Commun. 102 (2019) 203–209.
[46] S. Wang, J. Cao, W. Cui, L. Fan, X. Li, D. Li, Constructing chinky zinc oxide hierarchical hexahedrons for highly sensitive formaldehyde gas detection, J. Alloys Compd. 775 (2019) 402–410.
[47] M. Zhao, X. Ren, W. Pan, Mechanical and thermal properties of simultaneously substituted pyrochlore compounds $(Ca_2Nb_2O_7)_x$ $(Gd_2Zr_2O_7)_{1-x}$, J. Eur. Ceram. Soc. 35 (2015) 1055–1061.
[48] A. Sinha, B. Sharma, P. Gopalan, Development of novel perovskite based oxide ion conductor, Electrochim. Acta 51 (2006) 1184–1193.
[49] B. Mandal, N. Garg, S. Sharma, A. Tyagi, Solubility of ThO_2 in $Gd_2Zr_2O_7$ pyrochlore: XRD, SEM and Raman spectroscopic studies, J. Nucl. Mater. 392 (2009) 95–99.
[50] D. Han, K. Shinoda, S. Sato, M. Majima, T. Uda, Correlation between electro-conductive and structural properties of proton conductive acceptor-doped barium zirconate, J. Mater. Chem. A 3 (2014) 1243–1250.
[51] T. Gilbile, R. Pawar, V. Kapatkar, R. Kamble, S. Pawar, Synthesis and performance tuning of $Sm_{0.2}Ce_{0.8}O_{2-}\delta$ electrolyte for low temperature solid oxide fuel cell application, J. Electron. Mater. 48 (2019) 4117–4124.
[52] N. Miura, G. Lu, M. Ono, N. Yamazoe, Selective detection of NO by using an amperometric sensor based on stabilized zirconia and oxide electrode, Solid State Ion. 117 (1999) 283–290.
[53] N. Miura, T. Sato, S.A. Anggraini, H. Ikeda, S. Zhuiykov, A review of mixed-potential type zirconia-based gas sensors, Ionics 20 (2014) 901–925.
[54] G. Lu, N. Miura, N. Yamazoe, Stabilized zirconia-based sensors using WO_3 electrode for detection of NO or NO_2, Sens. Actuators B Chem. 65 (2000) 125–127.
[55] F. Zhong, L. Shi, J. Zhao, G. Cai, Y. Zheng, Y. Xiao, J. Long, Ce incorporated pyrochlore $Pr_2Zr_2O_7$ solid electrolytes for enhanced mild-temperature NO_2 sensing, Sens. Actuators B Chem. 43 (2017) 11799–11806.

Li Jiang received the B.Eng. degree in department of electronic science and technology in 2019. He is currently studying for his M.E. Sci. degree in College of Electronic Science and Engineering, Jilin University, China.

Caileng Wang received the B.S. degree in department of electronic science and technology in 2018. She is currently studying for her M.E. Sci. degree in College of Electronic Science and Engineering, Jilin University, China.

Jing Wang received her B.S. degree in applied chemistry in 2009 and the M.S. degree in polymer chemistry and physics in 2012 from Northeast Forestry University in China. Her current research is solid electrolyte gas sensor.

Fangmeng Liu received his PhD degree in 2017 from College of Electronic Science and Engineering, Jilin University, China. Now he is a lecturer of Jilin University, China. His current research interests include the application of functional materials and development of solid state electrochemical gas sensor and flexible device.

Rui You received his B.S. degree from Department of Opto-Electronic Engineering in 2013, Changchun University of Science and Technology, Changchun, China. He is now a Ph.D. student at the Department of Precision Instrument at Tsinghua University, Beijing, China. Currently his research interests mainly include gas sensor and application of MEMS process.

Siyuan Lv entered Jilin University in 2016. Now she is studying for her B.Eng. degree in department of electronic science and technology.

Guoyan Zeng entered Jilin University in 2017. Now he is studying electronic science and technology for his B.Eng. degree in college of electronic science and engineering.

Zijie Yang received the B.S. degree in department of electronic science and technology in 2017. He is currently studying for his M.E. Sci. degree in College of Electronic Science and Engineering, Jilin University, China.

Junming He received the B.Eng. degree in department of electronic science and technology in 2017. She is currently studying for her M.E. Sci. degree in College of Electronic Science and Engineering, Jilin University, China.

Ao Liu received the B.Eng. degree in department of electronic science and technology in 2018. He is currently studying for his M.E. Sci. degree in College of Electronic Science and Engineering, Jilin University, China.

Xu Yan received his M.S. degree in 2013 from Nanjing Agricultural University. He joined the group of Prof. Xingguang Su at Jilin University and received his Ph.D. degree in June 2017. Since then, he did postdoctoral work with Prof. Geyu Lu. Currently, his research interests mainly focus on the development of the functional nanomaterials for chem/bio sensors.

Peng Sun received his PhD degree from the Electronics Science and Engineering department, Jilin University, China in 2014. Now, he is engaged in the synthesis and characterization of the semiconducting functional materials and gas sensors.

Jie Zheng received the B.Sci. degree in 1984 from school of physics of Northeast Normal University in China and the M.S. degree in 1992 and the Dr. Eng. degree in 2002 from Changchun Institute of optics, Fine Mechanics and physics, Chinese Academy of Sciences. Now he is a professor at the College of Electronic Science and Engineering, Jilin University, China. He is engaged in the research of planar waveguides and fiber optic devices and their applications in sensors.

Geyu Lu received the B.Sci. degree in electronic sciences in 1985 and the M.S. degree in 1988 from Jilin University in China and the Dr. Eng. degree in 1998 from Kyushu University in Japan. Now he is a professor of Jilin University, China. His current research interests include the development of chemical sensors and the application of the function materials.